ADVANCED MATERIALS

DOI: 10.1002/adma.200501740

Highly Bendable, Transparent Thin-Film Transistors That Use Carbon-Nanotube-Based Conductors and Semiconductors with Elastomeric Dielectrics**

By *Qing Cao*, *Seung-Hyun Hur*, *Zheng-Tao Zhu*, *Yugang Sun*, *Congjun Wang*, *Matthew A. Meitl*, *Moonsub Shim*, and *John A. Rogers**

We report the use of networks of single-walled carbon nanotubes (SWNTs) with high and moderate coverages (measured as number of tubes per unit area) for all of the conducting (i.e., source, drain, and gate electrodes) and semiconducting layers, respectively, of a type of transparent, mechanically flexible, thin-film transistor (TFT). The devices are fabricated on plastic substrates using layer-by-layer transfer printing of SWNT networks grown using optimized chemical vapor deposition (CVD) procedures. The unique properties of the SWNT networks lead to electrical (e.g., good performance on plastic), optical (e.g., transparent at visible wavelengths), and mechanical (e.g., extremely bendable) characteristics in this "all-tube" TFT that would be difficult, or impossible, to achieve with conventional materials.

Invisible circuits based on transparent transistors have broad potential applications in consumer, military, and industrial electronic systems.[1,2] In backlit display devices, for example, transparent active-matrix circuits can increase the aperture ratio and battery life. Transparent electronic materials that can be printed on low-cost, flexible, plastic substrates are potentially important for new applications, such as bendable heads-up display devices, see-through structural health monitors, sensors, and steerable antennas.[3–5] More advanced systems, such as electronic artificial skins[6] and canopy window displays, will require materials that can also tolerate the high degrees of mechanical flexing (i.e., high strains) needed for integration with complex curvilinear surfaces.

Most examples of transparent TFTs (TTFTs) use thin films of inorganic oxides as the semiconducting and conducting layers.[7–9] Although the electrical properties of these oxides can be good (mobilities and conductivities as high as 20 $cm^2 V^{-1} s^{-1}$[10] and 4.8×10^3 $\Omega^{-1} cm^{-1}$,[11] respectively), their mechanical characteristics are not optimally suited for use in flexible and mechanically robust devices. For example, the tensile fracture strains for ZnO and indium tin oxide (ITO) thin films are less than 0.03 %[12] and 1 %,[13] respectively. Aligned arrays[14] or random networks[15,16] of individual SWNTs represent alternative classes of transparent semiconducting and conducting materials. In networks with high coverages of SWNTs, especially when in the form of small bundles, the metallic tubes (normally present with semiconducting tubes in a 1:2 ratio) form a percolating network that behaves like a conducting "film".[17,18] At moderate coverages, only the semiconducting tubes form such a percolating network and the film shows semiconducting properties.[19] Unlike the oxides, the SWNT films have excellent mechanical properties due to their high elastic moduli (1.36–1.76 TP nm/tube diameter nm)[20] and fracture stresses (100–150 GPa)[21] of the tubes. SWNT-based semiconductors have been used in flexible TFTs.[15,22–24] In one case, solution-deposited SWNT networks also formed the gate electrodes.[25] Although these TFTs can show good electrical properties, especially when CVD tubes are used,[24,26,27] the metal (Au, Pd, etc.) source, and drain electrodes limit their optical transparency and

[*] Prof. J. A. Rogers
Departments of Chemistry, Materials Science and Engineering, and Electrical and Computer Engineering
Beckman Institute
and Frederick Seitz Materials Research Laboratory
University of Illinois at Urbana-Champaign
Urbana, IL 61801 (USA)
E-mail: jrogers@uiuc.edu

Q. Cao
Department of Chemistry
Beckman Institute
and Frederick Seitz Materials Research Laboratory
University of Illinois at Urbana-Champaign
Urbana, IL 61801 (USA)

Dr. S.-H. Hur, Dr. Z.-T. Zhu, Dr. Y.-G. Sun, Dr. C.-J. Wang, M. A. Meitl
Department of Materials Science and Engineering
Beckman Institute
and Frederick Seitz Materials Research Laboratory
University of Illinois at Urbana-Champaign
Urbana, IL 61801 (USA)

Prof. M. Shim
Department of Materials Science and Engineering
University of Illinois at Urbana-Champaign
Urbana, IL 61801 (USA)

[**] We thank T. Banks for help with the processing and M. G. Xia for helpful discussions. This work was supported by DARPA-funded AFRL-managed Macroelectronics Program Contract FA8650-04-C-7101, the U. S. Department of Energy under grant DEFG02-91-ER45439, the NSF through grant NIRT-0403489, and a graduate fellowship from the Fannie and John Hertz Foundation (M. A. M.). Supporting Information is available online from Wiley InterScience or from the author.

mechanical flexibility (typical fracture strains for gold films are ~0.5 %[28]).

In this communication, the use of SWNT networks for all the conducting and semiconducting layers of TFTs is demonstrated. The devices use pristine networks with coverages ranging from several tubes to hundreds of tubes per square micrometer, grown by optimized CVD procedures on high-temperature substrates. Printing these network layers using dry-transfer techniques[24] one after another onto transparent plastic substrates and physically tough transparent dielectric layers yields highly bendable TTFTs. Analysis of the electrical, mechanical, and optical properties of the network films, the interfaces between them, and the resulting flexible TTFTs reveals unique characteristics that would be difficult, or impossible, to obtain with conventional materials.

Figure 1 shows a schematic illustration of the materials, device layouts, and fabrication procedures. Sheets of poly(ethyleneterephthalate) (PET; thickness ≈180 μm) served as transparent, flexible device substrates. Growth of SWNTs on a

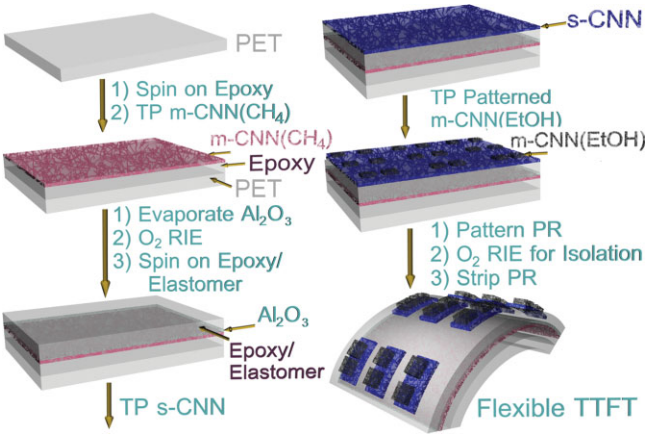

Figure 1. Schematic illustration of the materials, device layout, and fabrication procedures for mechanically flexible TTFTs that use SWNT networks for all of the active layers. The process involves CVD and transfer printing of SWNTs, to form the semiconducting and conducting layers of the devices. m-CNN and s-CNN refer to carbon nanotube networks that exhibit metallic and semiconducting properties, respectively. (EtOH) indicates a CVD procedure that uses a Fe/Co/Mo trimetallic catalyst loaded onto a high-surface-area silica support and ethanol feeding gas; (CH_4) indicates a similar growth procedure, but with methane as the feeding gas. The s-CNN layer was synthesized using CVD with a ferritin catalyst and methane feeding gas. TP refers to the transfer-printing process; RIE stands for reactive ion etching. PR: photoresist; PET: poly(ethyleneterephthalate).

SiO_2(100 nm)/Si wafer by CVD with a Fe/Co/Mo trimetallic catalyst[29] and methane (CH_4) feeding gas defined a metallic network (referred to as m-CNN(CH_4)) with moderately high coverage (~55 tubes μm^{-2}[30]). Transfer printing this m-CNN(CH_4) layer with an elastomeric stamp by use of a thin photocurable epoxy adhesive layer (SU8-2, Microchem Corp.) on the PET formed the gate electrodes of the TFTs. Devices were built using two different materials for the gate dielectric. One dielectric consisted of a spin-cast layer (thickness 1.5 μm) of the SU8-2 epoxy, which has mechanical properties comparable to other polymer electronic materials. The other dielectric was composed of a transfer-printed layer (thickness ≈2–4 μm) of the elastomer poly(dimethylsiloxane) (PDMS; Sylgard 184, Dow Corning),[31] which offers extremely high levels of elongation (greater than 100 %) before fracture, and a thin layer of epoxy spin-cast on top (thickness 300 nm) to promote adhesion of the SWNTs during transfer printing. In both cases, a thin layer of Al_2O_3 (thickness 100 nm) was deposited onto the m-CNN(CH_4) layer and then exposed briefly to O_2 plasma to promote wetting and adhesion of the epoxy and PDMS dielectrics. This layer was chosen to be sufficiently thick to protect the m-CNN(CH_4) layer from exposure to the plasma. A moderate-coverage CVD SWNT network (14 tubes μm^{-2}) provided the semiconducting network (referred to as s-CNN).[32] Transfer printing this s-CNN layer onto the surface of the gate dielectric defined the semiconductor layer of the TFTs. The dielectric thickness was selected to be much larger than the average spacing between the tubes in the m-CNN(CH_4) layer, to minimize spatial variations in the gate field at the semiconductor level. Calculations are provided in the Supporting Information. The source and drain electrodes used a high-coverage SWNT network (>200 tubes μm^{-2}, thickness ≈20–30 nm) grown on a SiO_2(100 nm)/Si substrate using procedures similar to those for the m-CNN(CH_4) layer, but with an ethanol (EtOH) feeding gas. Photolithography and oxygen-plasma etching on the growth substrate defined electrode patterns in this network (referred to as m-CNN-(EtOH)). Printing this patterned m-CNN(EtOH) layer onto the s-CNN layer formed source and drain electrodes electrically contacted to the semiconductor. Oxygen-plasma etching of the s-CNN through a photopatterned layer of photoresist electrically isolated individual TFTs and completed the fabrication process. We note that the printed CNN layers, in all cases, adhered well to the underlying materials. As a result, considerable processing, such as photolithography as described above, was possible without removing substantial numbers of SWNTs or significantly altering the properties of the networks.

Figure 2 shows scanning electron microscopy (SEM) images of each type of network after transfer printing onto a PET substrate. The uniformity in all cases is high, without any noticeable fluctuations in tube density over several square centimeters when the surface of the SiO_2/Si growth wafer was rendered hydrophilic with piranha-solution treatment before depositing the catalysts. The sheet resistances (R_s) of each type of SWNT network on PET were measured using a standard transfer-line model. The R_s values were ~265 ± 2 Ω square^{-1} and 9.5 ± 0.1 kΩ square^{-1} for the m-CNN(EtOH) and m-CNN(CH_4) films, respectively (see Supporting Information). To optimize the transistor transparency, we selected growth conditions for the m-CNN(EtOH) layer that would minimize the amount of amorphous carbon, multiwalled tubes, and bundles formed, by adjusting the ratio between ethanol and hydrogen. Similar optimization was carried out for the m-CNN(CH_4) layer. In this

ADVANCED MATERIALS

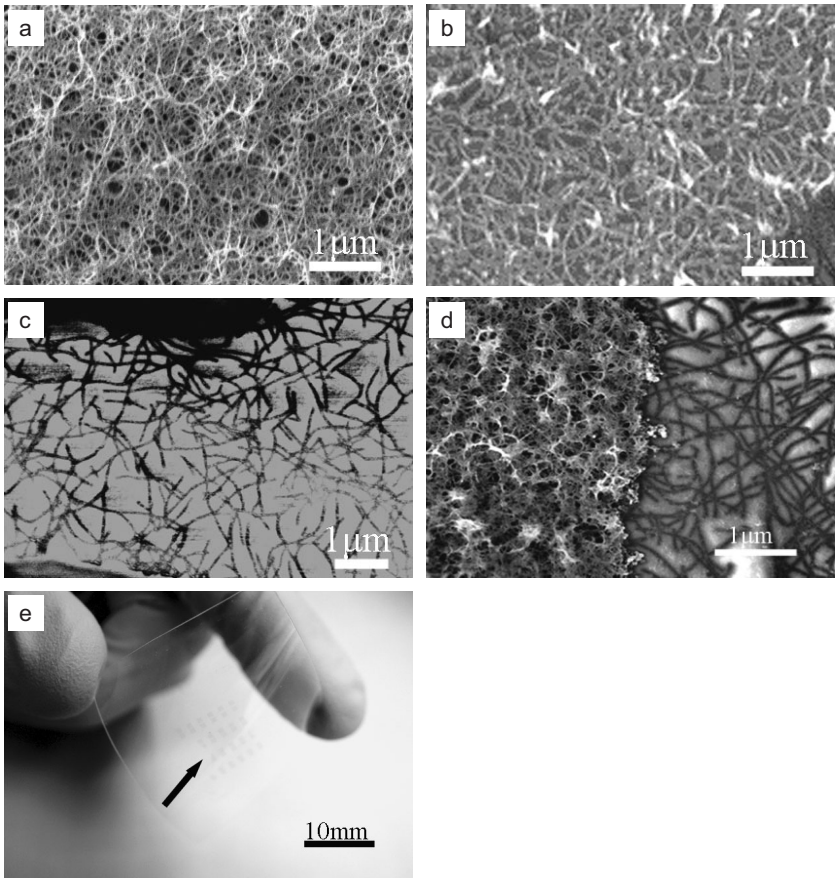

Figure 2. a–c) SEM images of SWNT networks that serve as source/drain electrodes (part a), gate electrodes (part b), and semiconductor layers (part c) in bendable TTFTs. d) SEM image of the interface between a source/drain electrode (left) and the semiconductor (right). e) Completed array of the "all-tube" TTFTs on a plastic substrate. The arrow indicates the source/drain structures which are slightly visible as arrays of grey squares in the center of this image.

case, however, we adjusted the coverage to be lower than that of the m-CNN(EtOH) layer to balance the degree of transparency and R_s, since modest conductivity in the gate electrode is acceptable for the individual device measurements presented here. Unlike the other films, R_s of the s-CNN layer could be modulated significantly using a gate electrode. The electrical properties of this layer were evaluated directly through measurements on the TFTs, as described in the following. The electrical properties of the interface between the source/drain electrodes and the semiconductor are critically important to device operation. Figure 2d shows an SEM image of the boundary between an m-CNN(EtOH) electrode (left) and a s-CNN film (right) (the apparent differences in tube diameters in the m-CNN(EtOH) and s-CNN films are artifacts of the SEM imaging and result from differences in the charging behavior in these two networks). Scaling studies, described subsequently, indicate that the contact resistance associated with this interface is negligible for the operation of devices studied here. The bottom frame of Figure 2 shows an array of completed TTFTs, which can be seen faintly in the center of this image as arrays of grey squares.

Figure 3 presents electrical characteristics of all-tube TTFTs that use epoxy dielectrics. In all cases, the devices operate in p-channel enhancement mode, and have leakage currents <5 nA. The effective device mobilities are between 26 and 30 $cm^2 V^{-1} s^{-1}$, as evaluated by applying the Shockley model to the transfer curves of Figure 3a.[27] Gate capacitances, C_i, are given by

$$C_i = \left(\frac{1}{C_{Al_2O_3}} + \frac{1}{C_{SU8-2}}\right)^{-1} = \left(\frac{d_{Al_2O_3}}{\varepsilon_{Al_2O_3}} + \frac{d_{SU8-2}}{\varepsilon_{SU8-2}}\right)^{-1} = 2.3 \text{ nF cm}^{-2} \quad (1)$$

where C_x, d_x, and ε_x ($x = Al_2O_3$, SU8-2) are the capacitances, thicknesses, and dielectric constants, respectively, of the Al_2O_3/SU8-2. This expression for the gate capacitance considers only the geometric properties and the material dielectric constants; it does not take into account fringing fields.[33] Figure 3b shows the current–voltage characteristics of a device with channel length, $L = 225$ μm in the linear-response regime. Figure 3c summarizes the mobilities and on/off ratios. We fabricated five different device arrays on plastic substrates. Each

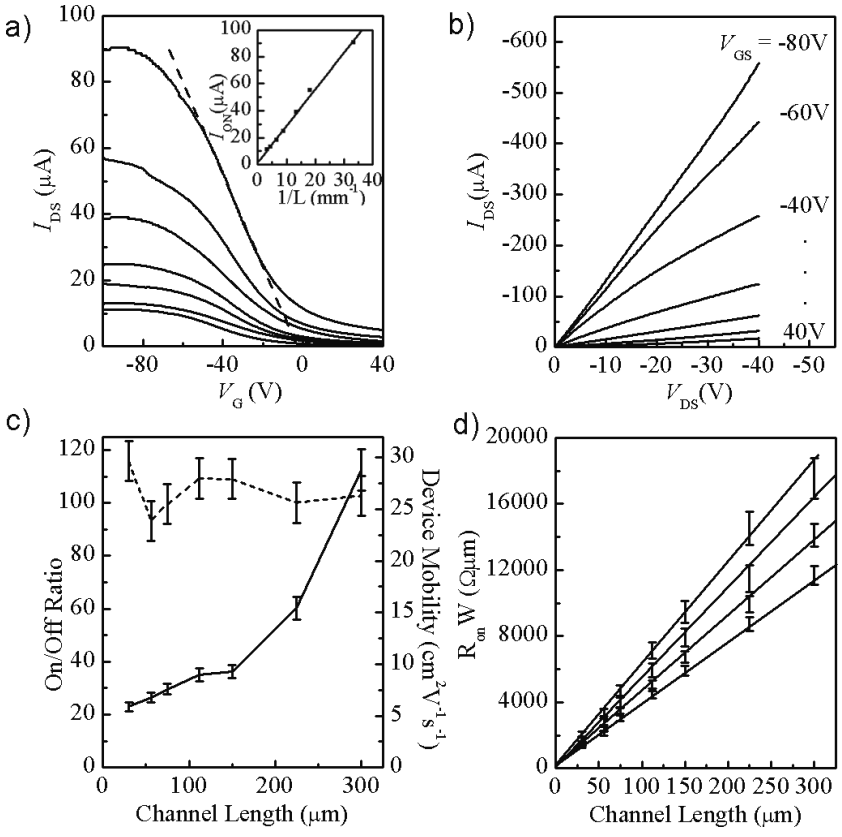

Figure 3. a) Transfer characteristics of all-tube TTFTs with different channel lengths (L). The channel widths were 750 μm and the drain/source voltage (V_{DS}) was –1.0 V in all cases. The channel lengths were 30, 55, 75, 112, 150, 225, and 300 μm from the top to the bottom, respectively. The dashed line indicates the slope used for determining the mobility for, as an example, the L = 30 μm device. Inset: On current (I_{ON}) versus the reciprocal of channel length ($1/L$). b) Current–voltage characteristics of a TTFT with a 750 μm channel width and a 225 μm channel length (gate voltage, V_{GS}: –80 to 40 V from top to bottom; 20 V steps). c) Effective device mobilities (dashed line, right axis) and on/off ratios (solid line, left axis) as a function of channel length. d) Width-normalized channel resistance as a function of channel length at different gate voltages (V_{GS}: –45 to –30 V from top to bottom; 5 V steps).

array consisted of 24 transistors with different channel lengths. We observed yields of ~80 % with all failed devices due to gate leakage. The mobilities of devices with identical geometries in a given array were the same to within ~5 %; variations of ~20 % were observed in devices measured on different arrays generated in different fabrication cycles. We did not observe any degradation in device characteristics over several months of storage in open air. The on/off ratios are modest because of the finite sheet resistance of the s-CNN layer, and they decrease with channel length as the probability of purely metallic pathways from source to drain increases. Chemical[34–36] and electrical[27] techniques can increase the on/off ratios by eliminating conduction through the metallic tubes.

The L-independent mobility values (Fig. 3c) and the linear scaling of on-current with $1/L$ (Fig. 3a, inset) are both consistent with semiconductor/electrode contacts that have negligible effects on device performance in this range of channel lengths. We also performed a scaling analysis by evaluating the channel resistance as a function of channel length and gate voltage, in the linear regime[37] (see Fig. 3d). The contact resistances, as determined from the y-axis intercepts of linear fits to the data, are negligible for all the channel lengths and gate voltages studied here, when compared to the channel resistances. This small resistance suggests good electrical contacts between the printed CNN layers. At the interface, each SWNT in the s-CNN layer is contacted to hundreds of metallic tubes in the m-CNN(EtOH) layer. Even with substantial tunnel and Schottky barriers between semiconducting and metallic tubes,[38,39] the overall contact resistance between the networks is low. The unipolar p-channel operation suggests that the Fermi level of the metallic tubes is not at the center of that of the semiconducting tubes[40] in spite of their similar graphene-like band structure, which is consistent with photoemission electron microscopy measurements.[41]

Figure 4 presents transmission spectra in the visible range of the electromagnetic spectrum for the PET substrate and the source/drain region of a completed TTFT. The data are not corrected for reflection losses. The transmittance of the source/drain region of the completed TTFT is ~80 % or larger in the visible region, which is only slightly less than the 85 % transmittance of the bare PET substrate. The absorbance of the m-CNN(CH_4), s-CNN films, and dielectrics are all negligible compared to that of the m-CNN(EtOH) layer. The

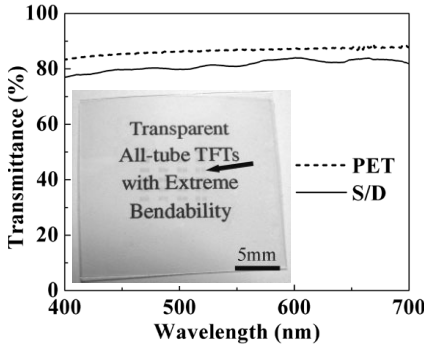

Figure 4. Optical transmittance as a function of wavelength for the PET substrate and the entire TTFT structure (including substrate) through the source/drain region. Inset: The arrow highlights one TTFT in an array of such devices formed on a sheet of PET that rests on top of a sheet of paper with printed text.

ADVANCED MATERIALS

level of transparency in these devices is comparable to some of the best TTFTs that use semiconducting and conducting oxides.[8,10] Furthermore, the SWNT devices show less variation in transmittance with wavelength than ITO. This neutral color response represents an advantage for display applications. Note here that the bandgap of the SWNTs (0.5–0.7 eV for 1–1.5 nm semiconducting SWNTs[40]) is much smaller than those of the oxides (>3 eV[1]). The transparency of the SWNT networks derives not from a large bandgap, but from i) a low, polarization-dependent, optical absorption cross section that results from the small size and highly anisotropic shape of the tubes;[42] ii) low carrier density in the SWNTs,[17] which results in low plasma frequency; and iii) high intrinsic mobilities and conductivities of SWNTs, such that even relatively low-coverage films (estimated at 10–25 % by area for the least-transparent m-CNN(EtOH) layer) provide good electrical properties.

The bending properties of these devices are also very good, in part due to the excellent mechanical properties of the SWNTs.[43,44] Figure 5 shows some results of bending tests, using previously described systems to induce tensile strains,[45] for devices that use epoxy dielectrics. Relatively small changes

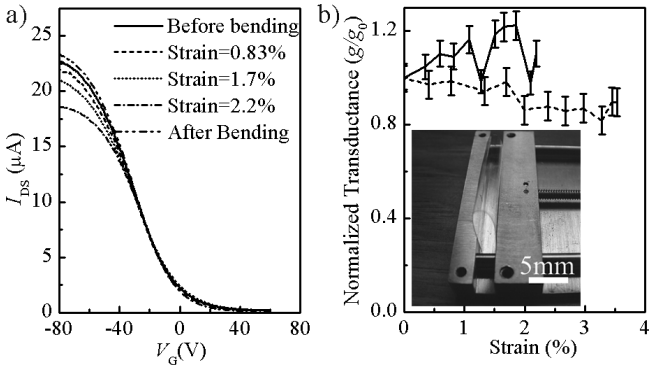

Figure 5. a) Transfer characteristics of a SWNT TTFT whose channel length and width are 225 and 750 μm, respectively, as measured before bending, at weak (0.83 %), moderate (1.7 %), and strong bending (2.2 %), and after bending. b) The change of normalized transconductance g/g_0 for transistors with an epoxy (solid line) and PDMS (dashed line) dielectric layer versus strain. Inset: Image showing the extremely high levels of bending that can be achieved with all-tube TTFTs that use PDMS gate dielectrics.

were observed in the transfer characteristics (Fig. 5a) and normalized transconductance (Fig. 5c) during bending up to tensile strains of 2 % with complete recovery after relaxing. The decrease of source/drain current may be caused by the enhanced electron scattering from strain-induced defects in the SWNTs.[43,46] These tensile strains exceed the fracture strains of other semiconductors that have been used for flexible TFTs, including microstructured Si and GaAs (1.4 and 1.2 %, respectively),[45,47] polysilicon (1–2 %),[48] and pentacene (1.4 %).[49] At strains larger than ~2 % the devices that use epoxy dielectrics fail irreversibly due to the emergence of large currents between source/drain and gate. We infer that failure of the dielectric, due to cracking, causes this behavior. By using PDMS as a physically tough elastomeric dielectric, it was possible to operate the devices successfully up to tensile strains of 3.5 % (see Supporting Information). This level of strain causes significant plastic deformation in the PET substrate. Even in these devices, failure occurs due to the appearance of large gate-leakage currents, rather than to electrical discontinuities in the SWNT networks. This result suggests that improved materials for the substrate and dielectric could enable even higher degrees of flexibility than those reported here.

In summary, transparent and flexible TFTs with good electrical properties can be realized with transfer printing CVD SWNT networks for use as the source/drain and gate electrodes, and semiconducting channel. When implemented with elastomeric dielectrics and flexible plastic substrates, these devices show extremely high degrees of flexibility. The main drawbacks of TFTs of this type are the moderate-to-low on/off ratios that occur in devices with high mobilities. Emerging chemical and electrical approaches appear promising for increasing the on/off ratios by selectively eliminating metallic pathways through the s-CNN layers.[27,34–36] As a result, we believe that these types of SWNT-based thin-film electronic materials will be important. Devices that use them have the potential to offer levels of electrical, optical, and mechanical performance that cannot be realized using known approaches.

Experimental

Synthesis of m-CNNs: The catalyst solution was made by loading iron acetate (6 mg, 99.995 % Aldrich), cobalt acetate (9 mg, 99.995 % Aldrich), and molybdenum acetate dimer (1.5 mg, 99 % Aldrich) into a 40 mL silica (100 mg, S5130 Sigma) ethanol suspension. The catalyst solution was spin-cast (3000 rpm, 1 min) onto a Si wafer with 100 nm thermal oxide which had been treated by piranha solution for 10 min. This catalyst was reduced with H_2 flow at 2400 sccm and 840 °C. SWNTs were grown with CH_4 flow at 2350 sccm and H_2 at 70 sccm for 20 min at 840 °C to generate the m-CNN(CH_4) layers. Growing SWNTs at 840 °C with H_2 flow at 10 sccm and Ar flow at 100 sccm passing through anhydrous ethanol in an ice bath for 30 min produced the m-CNN(EtOH) layers.

Synthesis of s-CNNs: Ferritin catalyst (Aldrich) diluted by deionized water at a volumetric ratio of 1:20 was deposited with methanol onto SiO_2(100 nm)/Si wafer pretreated by piranha solution. The catalyst was oxidized by heating the substrate to 800 °C in the air. Reducing with H_2 flow at 70 sccm and 900 °C followed by growing with CH_4 flow at 2500 sccm and H_2 at 70 sccm for 10 min at 900 °C yielded the s-CNN film.

Instrumentation: SEM images were taken with Hitachi S-4700 scanning electron microscope. Electrical characterizations were performed by current–voltage measurements using a semiconductor parameter analyzer (Agilent 4155C). UV–vis spectra were recorded by an Agilent 8453 spectrometer. The film thicknesses for all the dielectric materials and for the m-CNN (EtOH) layer were measured by a profilometer (Dektak 3030).

Received: August 19, 2005
Final version: October 23, 2005
Published online: January 3, 2006

[1] G. Thomas, *Nature* **1997**, *389*, 907.
[2] J. F. Wager, *Science* **2003**, *300*, 1245.
[3] S. R. Forrest, *Nature* **2004**, *428*, 911.

[4] R. H. Reuss, B. R. Chalamala, A. Moussessian, M. G. Kane, A. Kumar, D. C. Zhang, J. A. Rogers, M. Hatalis, D. Temple, G. Moddel, B. J. Eliasson, M. J. Estes, J. Kunze, E. S. Handy, E. S. Harmon, D. B. Salzman, J. M. Woodall, M. A. Alam, J. Y. Murthy, S. C. Jacobsen, M. Olivier, D. Markus, P. M. Campbell, E. Snow, *Proc. IEEE* **2005**, *93*, 1239.
[5] H. C. Lim, B. Schulkin, M. J. Pulickal, S. Liu, R. Petrova, G. Thomas, S. Wagner, K. Sidhu, J. F. Federici, *Sens. Actuators A* **2005**, *119*, 332.
[6] T. Someya, T. Sekitani, S. Iba, Y. Kato, H. Kawaguchi, T. Sakurai, *Proc. Natl. Acad. Sci. USA* **2004**, *101*, 9966.
[7] R. L. Hoffman, B. J. Norris, J. F. Wager, *Appl. Phys. Lett.* **2003**, *82*, 733.
[8] K. Nomura, H. Ohta, K. Ueda, T. Kamiya, M. Hirano, H. Hosono, *Science* **2003**, *300*, 1269.
[9] K. Nomura, H. Ohta, A. Takagi, T. Kamiya, M. Hirano, H. Hosono, *Nature* **2004**, *432*, 488.
[10] E. Fortunato, P. Barquinha, A. Pimentel, A. Goncalves, A. Marques, L. Pereira, R. Martins, *Adv. Mater.* **2005**, *17*, 590.
[11] R. Mamazza, D. L. Morel, C. S. Ferekides, *Thin Solid Films* **2005**, *484*, 26.
[12] C. W. Ong, D. G. Zong, M. Aravind, C. L. Choy, *J. Mater. Res.* **2003**, *18*, 2464.
[13] Y. Leterrier, L. Medico, F. Demarco, J.-A. E. Manson, U. Betz, M. F. Escola, M. Kharrazi Olsson, F. Atamny, *Thin Solid Films* **2004**, *460*, 156.
[14] C. Kocabas, S.-H. Hur, A. Gaur, M. A. Meitl, M. Shim, J. A. Rogers, *Small* **2005**, *1*, 1110.
[15] E. S. Snow, J. P. Novak, M. D. Lay, E. H. Houser, F. K. Perkins, P. M. Campbell, *J. Vac. Sci. Technol. B* **2004**, *22*, 1990.
[16] M. Kaempgen, G. S. Duesberg, S. Roth, *Appl. Surf. Sci.* **2005**, *252*, 425.
[17] Z. Wu, Z. Chen, X. Du, J. M. Logan, J. Sippel, M. Nikolou, K. Kamaras, J. R. Reynolds, D. B. Tanner, A. F. Hebard, A. G. Rinzler, *Science* **2004**, *305*, 1273.
[18] B. Vigolo, C. Coulon, M. Maugey, C. Zakri, P. Poulin, *Science* **2005**, *309*, 920.
[19] S. Kumar, J. Y. Murthy, M. A. Alam, *Phys. Rev. Lett.* **2005**, *95*, 066 802.
[20] B. Yakobson, P. Avouris, *Top. Appl. Phys.* **2001**, *80*, 287.
[21] M. R. Falvo, G. J. Clary, R. M. Taylor, V. Chi, F. P. Brooks, S. Washburn, R. Superfine, *Nature* **1997**, *389*, 582.
[22] K. Bradley, J. C. P. Gabriel, G. Gruner, *Nano Lett.* **2003**, *3*, 1353.
[23] S.-H. Hur, C. Kocabas, A. Gaur, M. Shim, O. O. Park, J. A. Rogers, *J. Appl. Phys.* **2005**, *98*, 114 302.
[24] S.-H. Hur, O. O. Park, J. A. Rogers, *Appl. Phys. Lett.* **2005**, *86*, 243 502.
[25] E. Artukovic, M. Kaempgen, D. Hecht, S. Roth, G. Gruner, *Nano Lett.* **2005**, *5*, 757.
[26] R. Seidel, A. P. Graham, E. Unger, G. S. Duesberg, M. Liebau, W. Steinhoegl, F. Kreupl, W. Hoenlein, *Nano Lett.* **2004**, *4*, 831.
[27] Y. Zhou, A. Gaur, S.-H. Hur, C. Kocabas, M. A. Meitl, M. Shim, J. A. Rogers, *Nano Lett.* **2004**, *4*, 2031.
[28] T. P. Weihs, S. Hong, J. C. Bravman, W. D. Nix, *J. Mater. Res.* **1988**, *3*, 931.
[29] G. Y. Zhang, D. Mann, L. Zhang, A. Javey, Y. M. Li, E. Yenilmez, Q. Wang, J. P. McVittie, Y. Nishi, J. Gibbons, H. J. Dai, *Proc. Natl. Acad. Sci. USA* **2005**, *102*, 16 141.
[30] The tube coverage was quantified by averaging the number of tubes extending into each 1 μm × 1 μm square in a 5 μm × 5 μm area in the SEM images.
[31] V. C. Sundar, J. Zaumseil, V. Podzorov, E. Menard, R. L. Willett, T. Someya, M. E. Gershenson, J. A. Rogers, *Science* **2004**, *303*, 1644.
[32] Y. Li, W. Kim, Y. Zhang, M. Rolandi, D. Wang, H. Dai, *J. Phys. Chem. B* **2001**, *105*, 11 424.
[33] D. V. Singh, K. A. Jenkins, J. Appenzeller, *Electron. Lett.* **2005**, *41*, 280.
[34] K. Balasubramanian, M. Friedrich, C. Jiang, Y. Fan, A. Mews, M. Burghard, K. Kern, *Adv. Mater.* **2003**, *15*, 1515.
[35] L. An, Q. Fu, C. Lu, J. Liu, *J. Am. Chem. Soc.* **2004**, *126*, 10 520.
[36] C. Wang, Q. Cao, T. Ozel, A. Gaur, J. A. Rogers, M. Shim, *J. Am. Chem. Soc.* **2005**, *127*, 11 460.
[37] S. Luan, G. W. Neudeck, *J. Appl. Phys.* **1992**, *72*, 766.
[38] M. S. Fuhrer, J. Nygard, L. Shih, M. Forero, Y. G. Yoon, M. S. C. Mazzoni, H. J. Choi, J. Ihm, S. G. Louie, A. Zettl, P. L. McEuen, *Science* **2000**, *288*, 494.
[39] A. A. Odintsov, *Phys. Rev. Lett.* **2000**, *85*, 150.
[40] S. Heinze, J. Tersoff, R. Martel, V. Derycke, J. Appenzeller, P. Avouris, *Phys. Rev. Lett.* **2002**, *89*, 106 801.
[41] S. Suzuki, Y. Watanabe, Y. Homma, S.-Y. Fukuba, S. Heun, A. Locatelli, *Appl. Phys. Lett.* **2004**, *85*, 127.
[42] M. F. Islam, D. E. Milkie, C. L. Kane, A. G. Yodh, J. M. Kikkawa, *Phys. Rev. Lett.* **2004**, *93*, 037 404.
[43] D. Bozovic, M. Bockrath, J. H. Hafner, C. M. Lieber, H. Park, M. Tinkham, *Phys. Rev. B* **2003**, *67*, 033 407.
[44] M. Motta, Y.-L. Li, I. Kinloch, A. Windle, *Nano Lett.* **2005**, *5*, 1529.
[45] E. Menard, R. G. Nuzzo, J. A. Rogers, *Appl. Phys. Lett.* **2005**, *86*, 093 507.
[46] S. B. Cronin, A. K. Swan, M. S. Unlu, B. B. Goldberg, M. S. Dresselhaus, M. Tinkham, *Phys. Rev. Lett.* **2004**, *93*, 167 401.
[47] Y. Sun, S. Kim, I. Adesida, J. A. Rogers, *Appl. Phys. Lett.* **2005**, *87*, 083 501.
[48] I. Chasiotis, *IEEE Trans. Device Mater. Reliab.* **2004**, *4*, 176.
[49] T. Sekitani, Y. Kato, S. Iba, H. Shinaoka, T. Someya, *Appl. Phys. Lett.* **2005**, *86*, 073 511.